Primary Current Distribution Model for Electrochemical Etching of Silicon Through a Circular Opening

A. Ivanov*[1], and U. Mescheder[1]
[1]Furtwangen University, Institute for applied research
*Corresponding author: Robert-Gerwig-Platz 1, 78120 Furtwangen, Germany, iva@hs-furtwangen.de

Abstract: Primary current distribution model for anodization of low-doped *p*-type silicon through a circular opening in frontside insulating mask is developed. The model is applied in two regimes of the process – pore formation and electropolishing – by definition of current density dependent functions of porosity and dissolution valence based on experimental results. As found also experimentally, transformation of etch forms from convex to concave occurring at specific etch depths are simulated using the model. The depth, at which this shape transformation occurred, is approximately twice larger in the model than in the experiment, which is assumed to be the result of using the simplified model with primary current distribution. Larger values of anisotropy were observed in the experiment than in the model.

Keywords: electrochemical etching, anodization, silicon, structuring, etch front movement.

1. Introduction

Anodization of silicon is an electrochemical process performed in fluoride electrolytes. Depending on the process conditions used – especially current density – the process results either in generation of porous silicon or electropolishing. The process was demonstrated as a flexible structuring technique to etch forms of various shapes [1, 2]. However, the process depends on many parameters, such as electrolyte concentration, silicon substrate doping and type, charge flow distribution, etc. [3]. Therefore it is challenging to transfer the process to industry scale. Modelling of the process, for example with COMSOL, can help bringing the process to a wider acceptance in industry. In the work presented here, etch form development observed in the anodization process through an insulating masking layer with a circular opening in galvanostatic regime was modeled and compared to experiments. The work is the further development, systematic analysis and corrections of the previously presented results [4, 5].

2. Theory

In electrochemical dissolution processes, amount of dissolved material and the dissolution rate is calculated from the Faraday's law of electrolysis with known current density, dissolution valence, and density and molar mass of the material. Thus, the etch rate is directly proportional to the local current density on the etch front. In case of silicon anodization in HF-based electrolytes, with increase of current density, the process switches from divalent reaction of pore formation (1) to tetravalent reaction of anodic oxidation (2) with subsequent etching of the oxide in reaction (3). With the reactions (2) and (3), silicon surface is electropolished.

$$\mathrm{Si} + 4\mathrm{HF_2^-} + \mathrm{h^+} \rightarrow \mathrm{SiF_6^{2-}} + 2\mathrm{HF} + \mathrm{H_2} + \mathrm{e^-} \quad (1)$$

$$\mathrm{Si} + 2\mathrm{H_2O} + 4\mathrm{h^+} \rightarrow \mathrm{SiO_2} + 4\mathrm{H^+} \quad (2)$$

$$\mathrm{SiO_2} + 2\mathrm{HF_2^-} + 2\mathrm{HF} \rightarrow \mathrm{SiF_6^{2-}} + 2\mathrm{H_2O} \quad (3)$$

In the transition of the process from pore formation to electropolishing, porosity of the generated porous silicon layer changes with increase of current density from, e.g., 70 % for *p*-type silicon of resistivity in the range 10–20 Ω cm anodized in 1:1 volume ratio of 50 m% HF and absolute ethanol, to 100 % in electropolishing regime, and must be also considered in the model.

In the primary current distribution, only resistivity of the materials (electrodes, electrolyte) is taken into account, neglecting activation and concentration overpotentials. Thus, it provides a rather simplified description of an electrochemical problem. Due to relative simplicity and ease of solving such a model, it is recommended as a first approximation of the problem [6].

3. Methods

3.1 Model

In the present work, primary current distribution model for the process was developed in COMSOL Multiphysics™ (COMSOL Inc., Burlington, USA), version 5.1, using the electrodeposition physics interface (*edsec*). In the following, the model description is given. Special terms of the COMSOL software are indicated with italicized text.

The 2D geometry of the models with axial symmetry consisted of the following domains (Fig. 1):

- electrolyte with conductivity of 34.11 S/m (corresponds to aqueous HF electrolyte with HF mass fraction in percent of 29.93 m% [7]);
- silicon substrate with conductivity 7.5 S/m as anode;
- empty region representing frontside insulating layer of silicon nitride (SiN) of thickness 1 µm on the silicon substrate with an opening of radius R_{open} (diameter D_{open}); thickness of SiN layer in the experiments was below 300 nm; value of 1 µm is used here in order to reduce number of mesh elements by avoiding very small features in the model geometry; the increased mask thickness of 1 µm is assumed to have no effect on the etch form development for the applied values of $R_{open} \geq 100$ µm;
- "predefined etch form" of thickness 5 µm for enhanced mesh movement; this domain belonged to the electrolyte region.

The geometry was built by a generation sequence of elementary shapes (*rectangles* and *polygons*), and Boolean operations (*difference* and *union*). The geometry was finalized as a union, meaning that adjacent domains shared same nodes on the boundaries. To improve stability of the model and reduce number of mesh nodes, *fillets* were applied to the right angles on the mask edge and the predefined etched form.

The etch front was described by the *depositing electrode surface* defined for the interfacial boundary between the electrolyte and silicon regions. For *electrode reaction*, current density dependent porosity and dissolution valence functions have been reconstructed for the model from experimental data (s. Fig. 2 and Fig. 3). These functions have been defined with

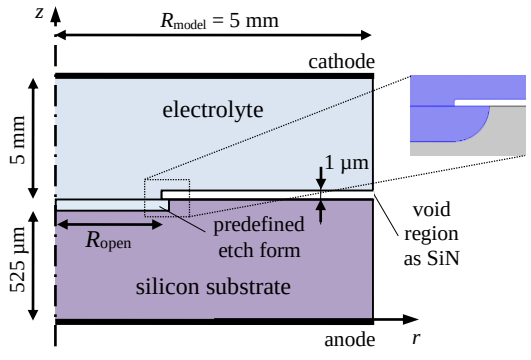

Figure 1. Schematic geometry of the model (not in scale) in 2D with symmetry axis at $r = 0$; varied opening radius R_{open} was applied.

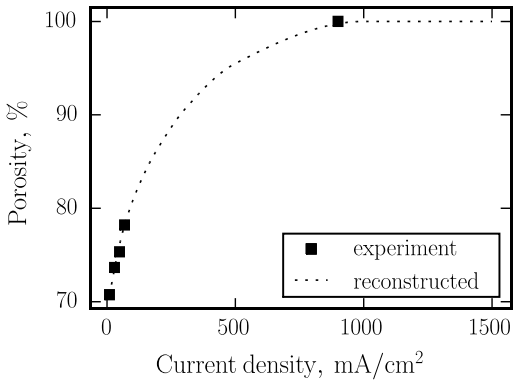

Figure 2. Dependence of porosity of porous silicon on current density for anodization of low doped silicon of resistivity in the range 10–20 Ω cm in 29.93 m% HF with ethanol (1:1 volume ratio of 50 m% HF and absolute ethanol) at room temperature.

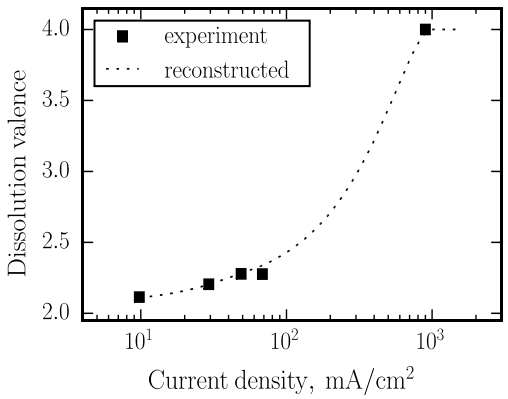

Figure 3. Dependence of dissolution valence on current density for anodization of silicon of resistivity in the range 10–20 Ω cm in 29.93 m% HF with ethanol (1:1 volume ratio of 50 m% HF and absolute ethanol) at room temperature.

interpolation functions with piecewise cubic interpolation and linear extrapolation. The dissolution valence was set in the *electrode reaction* node as *number of participating electrons* and reciprocal of the porosity was set as *stoichiometric coefficient*. The option *Solve for depositing species concentration* was deactivated, because the *edsec* interface was applied here for an etch process.

The case of low doped silicon and high-concentrated electrolyte results in a non-stable movement of the etch front, because a pit on the etch front introduced by noise (inaccuracy) of numerical calculations continues to grow, since the resistance of this electrical path reduces in comparison to neighboring spots. As a result, the moving boundary of the etch front in the first moments of the process transforms to a wavy surface, and the solver does not converge. To overcome this instability, the built-in *moving boundary smoothing* has to be applied.

All domains were meshed with *free triangular mesh*. The regions of the model were meshed separately, starting from the most important regions near the moving etch front boundary. Custom adjustments of the default parameters for *normal* mesh quality have been applied to improve stability of the mesh movement.

The model was solved for different radii of opening in the frontside insulating masking layer R_{open}, where R_{open} was ranging from 100 µm to 500 µm and different initial current densities j_{init} in the range 1.0–3.5 A/cm^2, resulting in the total current $I_{total} = j_{init}\,\pi R_{open}^2$. The electrical supply was defined as following: the lower boundary of the silicon domain (anode) was grounded, and inward electrolyte current density of $I_{total}/(\pi R_{model}^2)$ was set to the top boundary of the electrolyte domain (cathode).

In order to solve the model for large mesh movement (etch front movement up to the lower boundary of the 525 µm thick silicon substrate, Fig. 1), *automatic remeshing* was activated. The condition for remeshing was defined as square root of the maximum element distortion *edsec.I1isoMax* being above or equal to two.

The model results were saved for values of time in the range defined as {range(0, t_{step}, 200)}^3, where the t_{step} parameter was varied in order to achieve saving of 40–150 results. To improve solving, *non-linear method* was set *constant (Newton)* with *Jacobian update on every iteration*, and *consistent initialization* was activated.

Exported etch profiles were characterized by anisotropy factor and curvature at the bottom of structures. The evaluation was performed in custom scripts in Python programming language v.3.4.1 with Numpy library in the Spyder 2.3.1 programming environment.

Anisotropy factor A_f of an etch form of width w_{etch} and depth d_{etch} was calculated according to eq. (4):

$$A_f = 1 - \frac{0.5 w_{etch} - R_{open}}{d_{etch}} \qquad (4)$$

Curvature was evaluated by performing an arc fit to the central region of radius $0.4 w_{etch}$. The structure depth, at which the shape switched from convex (negative curvature) to concave (positive curvature) was called threshold depth d_{th}.

3.2 Experiment

In the experiment, low doped *p*-type silicon samples (10–20 Ω cm, (100)-Si, thickness approx. 525 µm) with multiple circular openings of different radii R_{open} in the range 100–500 µm in low stress SiN on top of silicon sample (s. Fig. 4) were used.

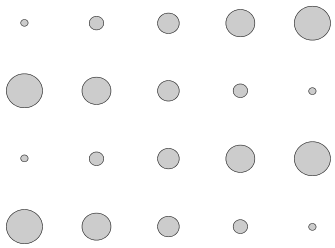

Figure 4. Layout of openings in frontside SiN layer on silicon samples used in the work, with radius varied from 100 µm to 500 µm and distance of 2 mm between the centers of the openings; total open area on a sample was 0.06912 cm^2 .

Double-tank cell with wet backside contact to the sample and two platinum electrodes was applied. The to be etched wafer separated the two tanks, thus allowing a well-controlled current density in the etched area. In order to provide an electrical (ohmic) contact, the backside of the samples was additionally doped with boron.

The samples were anodized at room temperature in 29.93 m% HF electrolyte prepared as 1:1 volume ratio of 50 m% HF and absolute ethanol.

Constant total current corresponding to initial current density j_{init} in the range 1.0–3.5 A/cm^2 (calculated for the total area of the openings on a sample of 0.06912 cm^2) was applied. Possible non-uniform distribution of charge between the openings resulting in different values of current density for each opening was assumed to be negligible. Anodization for etch duration of 1 min, 5 min, 10 min and 20 min (the latter only for j_{init} in the range 1.0–2.5 A/cm^2) was performed, resulting in 22 samples.

After removal of porous silicon in 1 m% KOH and SiN in buffered HF, 2D topographical scans of the etch forms were measured with Dektak 150 stylus profiler (Veeco Metrology, Tucson, USA). Etch forms have been characterized, similarly to the simulated forms, with anisotropy factor and curvature at the bottom evaluated with Python.

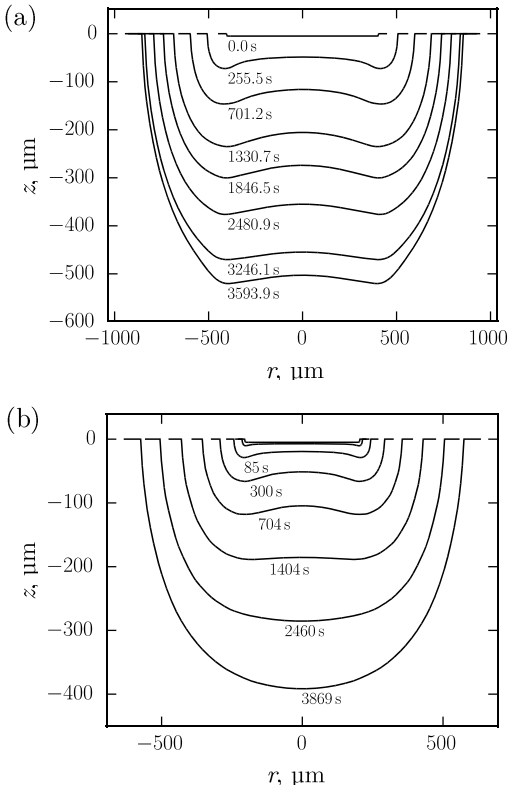

Figure 5. Simulated etch forms for diameter of opening (a) 800 µm and (b) 400 µm and initial current density of 1 A/cm^2.

4. Results

4.1 Simulation results

For diameter of opening of 200 µm and 400 µm, etch form development from convex form to concave was observed for all simulated initial current density values. For the bigger openings, only convex forms were obtained. As example, the resulting etch form development for diameter of the frontside opening of 400 µm and 800 µm and initial current density of 1 A/cm^2 is shown in Fig. 5.

Dependence of curvature at the bottom of etch profiles on structure depth for initial current density of 1 A/cm^2 is shown in Fig. 6. Similar curves were observed for all other values of initial current density. An amplification of the curvature value (i.e. convex shapes getting more convex and concave shape getting more concave) at depth above approximately 450 µm was observed in all cases.

Anisotropy factor as defined in (4) in dependence of structure depth for simulated etch forms for initial current density of 1 A/cm^2 is shown in Fig. 7. Curves for all other simulated values of initial current density are similar to the shown one and varied in the same range from approximately –0.6 to 0.25.

Threshold depth in dependence of diameter of opening for all simulated values of initial current density is shown in Fig. 8.

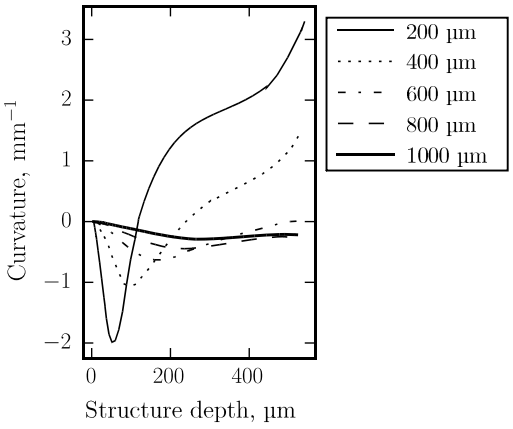

Figure 6. Curvature vs. structure depth for simulated etch forms for initial current density of 1 A/cm^2; the values in the keys are D_{open}.

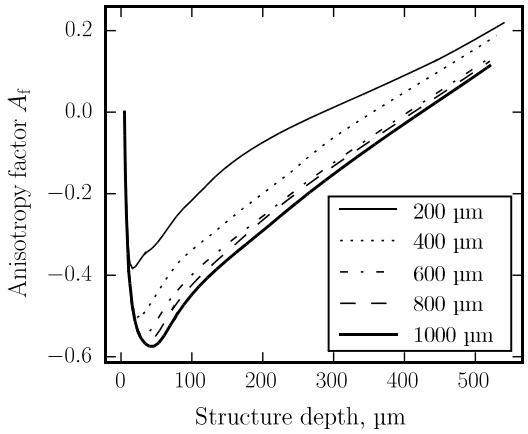

Figure 7. Anisotropy factor vs. structure depth for simulated etch forms for initial current density of 1 A/cm^2; the values in the keys are D_{open}.

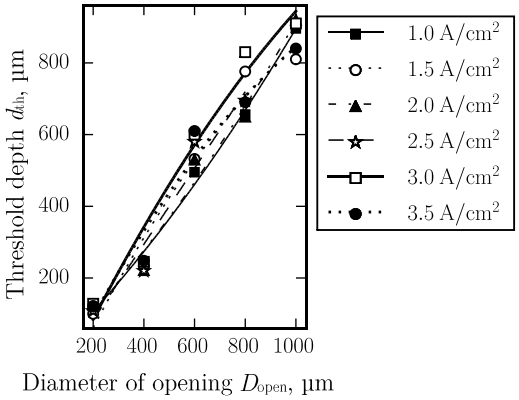

Figure 8. Threshold depth vs. diameter of opening evaluated from the simulated data; the datasets are for varied initial current density; the values of threshold depth above 500 µm were obtained by extrapolation of the curvature curves.

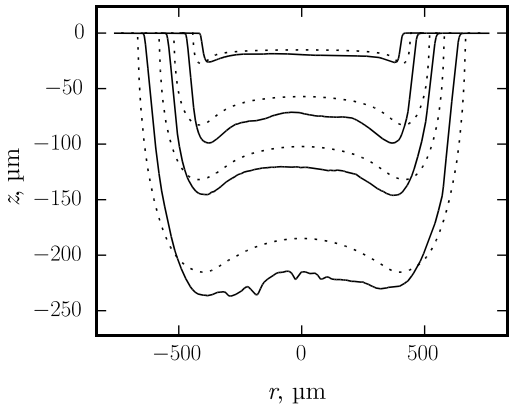

Figure 9. Comparison of the simulated etch profiles (dotted lines) and experimental etch profiles (solid lines) for diameter of opening of 800 µm and initial current density of 1 A/cm^2; the curves are for etch time of 1 min, 5 min, 10 min, and 20 min.

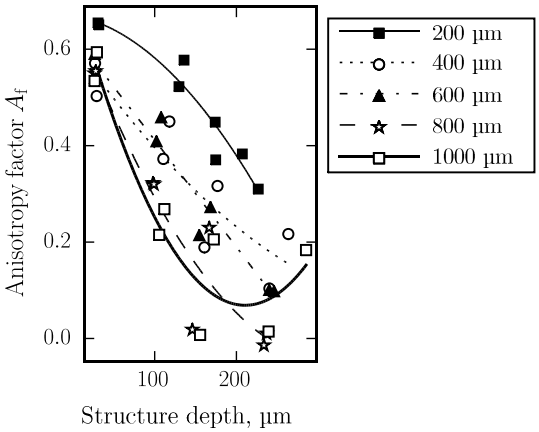

Figure 10. Anisotropy factor vs. structure depth for experimental etch forms for initial current density of 1 A/cm^2; the values in the keys are D_{open}.

4.2 Experimental results

Four different etch time values were used in the experiments (1 min, 5 min, 10 min, and 20 min), therefore not much data were available for comparison to the simulation. Nevertheless, we could evaluate some tendencies and compare them to the model.

As in the simulation, we did not observe transformation of shapes from convex to concave for all parameter combinations. For example, in Fig. 9, comparison of the simulated and experimental etch profiles for diameter of opening of 800 µm and initial current density of 1 A/cm^2 is shown.

Anisotropy factor dependence on structure depth was not equal for different values of initial current density. At 1 A/cm^2, anisotropy factor decreased with increase of structure depth from high positive values of approximately 0.7 to about zero (s. Fig. 10). With increase of initial current density up to 3.5 A/cm^2, the negative slope of anisotropy factor vs. depth reduced to about zero, with the anisotropy factor remaining at high positive values of about 0.4–0.7 even for increased depth.

Fig. 11 shows threshold depth in dependence of diameter of opening obtained for the experimental etch forms.

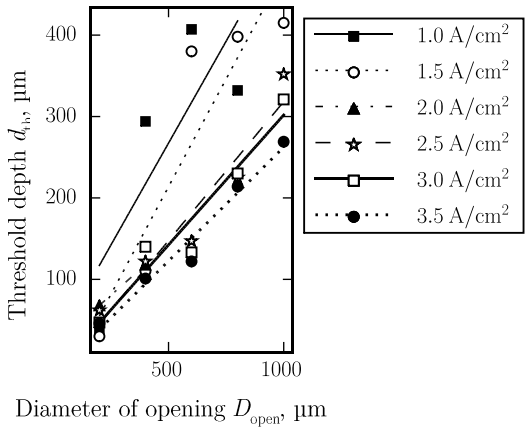

Figure 11. Threshold depth vs. diameter of opening evaluated for the experimental etch forms; the datasets are for varied initial current density.

5. Discussion

Comparison of the etched volume between the experiment and the simulation showed that the etched volume in the simulation in average is only 4 % larger than in the experiment. Thus, the chosen functions of porosity and dissolution valence applied in the model provided good results.

Transformation of etch forms from convex to concave was observed both in the experiment and the simulation. However, values of threshold depth evaluated from the simulation are approximately twice larger than the values from the experiment (compare Fig. 8 and Fig. 11). Additionally, in contrast to the experiment, in the simulation almost no dependence of the threshold depth values on initial current density was observed.

The comparison of the results revealed big difference between the values of anisotropy factor in the simulation and the experiment: In the experiment, anisotropy factor remained at large positive values of about 0.55–0.7 or decreased to zero with increase of structure depth. In the simulation, in contrast, anisotropy factor decreased strongly to large negative values in the beginning of the process (meaning lateral etch rate being much higher than vertical etch rate), and then gradually increased up to small positive values of about 0.2. Additionally, similarly to the curvature plots, only small dependence of the anisotropy factor curves on initial current density was observed in the simulation.

The pronounced discrepancies between simulation and experimental results are a strong indication that the model is a rather simplified model of the anodization process. As further development, activation overpotential has to be considered in the model (as done in secondary and tertiary current distribution models). By this we expect that the process becomes more isotropic, meaning reduction of absolute values of anisotropy. However, the large negative anisotropy factor values would be closer to 0, but presumably still negative. Moreover, one would not expect increase of anisotropy factor to large positive values in this case. However, with this improvement a better coincidence of simulation and experiments in respect to the threshold depth is expected, thus more isotropic process would likely result in smaller threshold depth values, bringing the model closer to the experiment.

Concentration polarization, used in tertiary current distribution, again, is expected to make the etch process more isotropic, thus could also not explain the discrepancies in the values of anisotropy factor, but could make threshold depth more comparable to the experiment.

Thus, activation and concentration polarization could result in a model more closely describing anodization process. However, there must be other factors for the large positive anisotropy factor observed in the experiment. For example, anisotropy could be induced by the crystal orientation of silicon samples. There are reports on crystallographic dependence of silicon anodization process: Lehmann observed difference between the values of critical current density (at which the process switches from pore formation to electropolishing) for n-type silicon samples of different crystallographic orientation [8]. Guendouz et al. for highly doped *p*-type silicon, and Tjerkstra for moderately doped *p*-type silicon, reported on evolution of pseudo V-shapes with sharp bottom [9, 10]. However, we did not observe this kind of shapes in our experiments. Nevertheless, in our experiment, we used only (100)-oriented samples; therefore, further study with other crystal orientation is necessary to check whether there is a crystallographic dependence of anisotropic factor for the chosen process conditions.

6. Conclusions

In this paper, primary current distribution model for anodization of low-doped *p*-type silicon through a circular opening in frontside insulating mask was developed and compared to experiment. The model includes both, pore formation and electropolishing regimes of the process.

The chosen porosity and valence functions for the model showed comparable results to the experiment in regard to etch volume.

The model showed transformation of etch forms from convex shape to concave as in the experiment. However, the values of threshold depth, at which this transformation occurred, in the simulation were approximately twice larger than in the experiment, which is assumed to be the result of the model lacking the activation and concentration polarization.

Much lower values of anisotropy obtained for the simulated etch forms could not be explained with the absence of the activation and concentration polarization. Instead, it is assumed that some other factor must play here a role, for example, dependence of the process on crystallographic orientation.

7. References

1. A. Ivanov et al., High quality 3D shapes by silicon anodization, *physica status solidi (a)*, **208**, 1383–1388 (2011)
2. A. Ivanov, U. Mescheder, Silicon Electro-chemical Etching for 3D Microforms with High Quality Surfaces, *Advances in Abrasive Technology XIV: Selected, peer reviewed papers from the 14th International Symposium of Advances in Abrasive Technology (ISAAT 2011), September 18-21, 2011, Stuttgart, Germany*, T Trans Tech Publications, 666–671 (2011)
3. V. Lehmann, *Electrochemistry of Silicon.* Wiley-VCH Verlag GmbH, Weinheim (2002)
4. A. Ivanov, U. Mescheder, Dynamic Simulation of Electrochemical Etching of Silicon with COMSOL, *Proceedings COMSOL Conference 2012, October 10-12, 2012, Milan (Italy)*, 7 pages (2012)
5. A. Ivanov et al., Finite-Elements Simulation of Etch Front Propagation in Silicon Electropolishing Process, *ECS Transactions*, **58**, 15–24 (2014)
6. M. Noessler, Which Current Distribution Interface Do I Use?, *COMSOL Blog*, available online http://www.comsol.com/blogs/current-distribution-interface-use/ (2014, accessed 01.09.2015)
7. E. Hill and A. Sirkar, The electric conductivity and density of solutions of hydrogen fluoride, *Proceedings of the Royal Society of London. Series A*, **vol. 83**, no. 560, pp. 130–148 (1909)
8. V. Lehmann, The physics of macropore formation in low doped n-type silicon, *Journal of the Electrochemical Society*, **vol. 140**, no. 10, pp. 2836–2843 (1993)
9. M. Guendouz, P. Joubert, and M. Sarret, Effect of crystallographic directions on porous silicon formation on patterned substrates, *Materials Science and Engineering: B*, **vol. 69**, pp. 43–47 (2000)
10. R. W. Tjerkstra, Isotropic etching of silicon in fluoride containing solutions as a tool for micromachining, *Ph.D. dissertation* (1999)

8. Acknowledgements

The study was performed in frames of the PhD work of A. Ivanov in Furtwangen University, supervised by Prof. Dr. U. Mescheder from Furtwangen University and Prof. Dr. P. Woias from University of Freiburg. The authors are thankful to the team of the micro-technological laboratory at Furtwangen University for support in the preparation of the samples.